Data requirements for a 5-mm quasi-geoid in the Netherlands

Farahani, Hassan H.; Klees, Roland; Slobbe, Cornelis

DOI
10.1007/s11200-016-0171-7

Publication date
2017

Document Version
Final published version

Published in
Studia Geophysica et Geodaetica: a journal of geophysics, geodesy, meteorology and climatology

Citation (APA)
Farahani, H. H., Klees, R., & Slobbe, C. (2017). Data requirements for a 5-mm quasi-geoid in the Netherlands. *Studia Geophysica et Geodaetica: a journal of geophysics, geodesy, meteorology and climatology*, *61*(4), 675–702 . https://doi.org/10.1007/s11200-016-0171-7

Data requirements for a 5-mm quasi-geoid in the Netherlands

HASSAN H. FARAHANI, ROLAND KLEES AND CORNELIS SLOBBE

Delft University of Technology, Stevinweg 1, 2628 CN Delft, The Netherlands
(h.hashemi@tudelft.nl)

Received: July 15, 2016; Revised: October 5, 2016; Accepted: January 19, 2017

ABSTRACT

We assess the surface gravity data requirements for a 5-mm quasi-geoid model for the Netherlands mainland and continental shelf in terms of omission and commission errors. The omission error critically depends on the roughness of the topography and bathymetry. For the Netherlands continental shelf, Central and Northern Netherlands, the omission error is well described by the model 0.32d mm, where d is the data spacing in km. For the more hilly Southern Netherlands, the omission error model is 0.92d mm. The commission error depends on the kernel modification, the data spacing, and the data accuracy. When using the spheroidal Stokes kernel, it is well described by 0.277 d $\sigma_{\Delta g}$ mm, where $\sigma_{\Delta g}$ is the noise standard deviation of surface gravity data in mGal. An upper bound of the commission error of the state-of-the-art satellite-only gravity model GOCO05S over the Netherlands is $e^{0.03676L-11.419}$ mm, where L is the maximum degree up to which this model is used. Only if this model is truncated at a sufficiently low degree, e.g., at degree 100, its contribution to the total commission error can be neglected. We determine the total error as the sum of commission and omission errors. Hence, to realize a 5-mm quasi-geoid model for the Netherlands mainland and continental shelf, a data spacing of 3.5 km is needed when assuming a noise standard deviation of 1.5 mGal for surface gravity data. The currently available land-based gravity data fulfill this requirement. This does not apply to the situation at sea, where the density of the shipboard gravity data and the accuracy of the radar altimeter-derived data do not allow the realization of a 5-mm quasi-geoid model.

Keywords: quasi-geoid, omission error, commission error

1. INTRODUCTION

Height networks belong to the geometric infrastructure of all countries worldwide. They consist of markers with known heights. Their main function is to give users access to height information. The need for such a network is driven by the primary measurement technique for heighting, spirit levelling, which is a relative measurement technique. If the height of one point is known, the height of another point is found by measuring the difference in heights with spirit levelling. Spirit levelling is one of the most accurate

measurement techniques and can provide information about height differences with an accuracy of below $1\,\mathrm{mm}\cdot\sqrt{K}$, where K is the levelling distance in km (*Vaníček et al., 1980*). Depending on the topography, corrections to levelled height differences are needed to guarantee that the height differences provide information about the direction of water flow (*Vaníček and Krakiwsky, 1986*).

The current practice of heighting is to use such height networks and perform spirit levelling to determine the heights of new markers. This approach has two major drawbacks. First, a height network marker may have moved in vertical direction, e.g., in response to various geophysical processes or due to anthropogenic activities. Hence, there is a need to frequently control the markers of the height network, and if changed, correct the heights. Second, spirit levelling is a time-consuming, hence costly, measurement technique. Both aspects make the current heighting approach quite expensive and, therefore, hardly sustainable. Already with the advent of Global Navigation Satellite Systems (GNSS), the use of GNSS for heighting has been discussed. Though GNSS-based heighting is also a relative measurement technique, the number of reference stations to be maintained is limited, observing them can be fully automatized, and the number of reference points is definitely much lower than the number of height markers. More importantly, GNSS-based heighting is less time-consuming, making it more cost effective compared to spirit levelling.

When physical heights are requested, a prerequisite of using GNSS for heighting is that the geoid or the quasi-geoid is known with sufficient accuracy, depending on whether orthometric or normal heights are used. Hence, an alternative to a height network in combination with spirit levelling as the primary measurement technique is to use the (quasi-) geoid as the height reference surface in combination with GNSS as the primary measurement technique. So far, the Netherlands and many other countries maintain their levelling networks and, at the same time, provide users with information about the (quasi-) geoid to allow for what is commonly referred to as GNSS levelling. Recently, the Canadian Spatial Reference Service (CSRS) decided to realize a new vertical datum by geoid modelling, rather than by spirit levelling, and to use GNSS as the primary measurement technique (*Véronneau and Huang, 2016*). Recently, a discussion has been initiated in the Netherlands about the future of the NAP (Normaal Amsterdams Peil) levelling network, which is driven by high costs for its maintenance and lower budgets for the maintenance of the geodetic infrastructure.

Whether or not a (quasi-) geoid model can serve as a height reference surface and GNSS as the measurement technique for heighting depends on the adopted user requirements, in particular, the accuracy. This depends on the accuracy of GNSS heights and the accuracy of the (quasi-) geoid model. Even for countries with an excellent gravity data coverage and quality as well as a flat topography and bathymetry, the accuracy of the (quasi-) geoid model is still considered as a critical factor in the realization of a GNSS-based height system.

The quality of a (quasi-) geoid model depends on many factors, among others, the data accuracy and spatial resolution, and the methodology used to compute the (quasi-) geoid model. Several studies have been done in the past to assess the surface gravity data requirements for the (quasi-) geoid modelling at different geographic areas and target

accuracies (*Kearsley, 1986*; *Forsberg, 1993*; *Jekeli et al., 2009*; *Jekeli, 2012*; *Ågren and Sjöberg, 2014*).

The main objective of this study is to assess the surface gravity data requirements for a 5-mm quasi-geoid model (68% confidence level) in terms of omission and commission errors for the Netherlands mainland and continental shelf. The commission error is caused by observational errors, which propagate into the quasi-geoid model. In that sense, it is mainly controlled by the measurement noise. The omission error ensues from a lack of spatial resolution in surface gravity data, i.e., it can be reduced only by improving the data density.

Four questions will be addressed in this study:

1. How does the omission error change as a function of the spatial resolution of the surface gravity data?
2. How large is the commission error as a function of the noise standard deviation of surface gravity data when assuming zero-mean white Gaussian noise?
3. What are the data requirements in terms of spatial resolution and accuracy for the realization of a 5-mm quasi-geoid for the Netherlands mainland and continental shelf?
4. To what extent do the currently available surface gravity data sets meet these requirements? If not, is there a data acquisition technique that is able to provide data with the required accuracy and density?

The paper is structured as follows. In Section 2, we describe the methodology and data used to estimate the omission error and analyse the results. In Section 3, we discuss the computation of the commission error and present the results of the computations. The total error, defined as the sum of omission and commission errors, is discussed in Section 4. Based on the results presented in Section 4, we evaluate in Section 5 whether or not the current data situation suffices to realize a 5-mm quasi-geoid model over the Netherlands mainland and continental shelf. Finally, in Section 6, we conclude by summarizing the main findings.

2. OMISSION ERROR

2.1. Background

The disturbing potential, which is defined as the difference between the Earth's gravity potential and the GRS80 normal gravity potential (*Moritz, 1984*), can be written in terms of spherical harmonics as (*Heiskanen and Moritz, 1967*)

$$T(\boldsymbol{x}) = \frac{GM}{a} \sum_{l=0}^{\infty} \sum_{m=-l}^{l} \bar{c}_{lm} \left(\frac{a}{|\boldsymbol{x}|} \right)^{l+1} \bar{Y}_{lm}(\hat{\boldsymbol{x}}) \ . \tag{1}$$

Herein, $\bar{Y}_{lm}$ is the 4π-normalized surface spherical harmonics of degree l and order m, $\bar{c}_{lm}$ is a spherical harmonic coefficient of degree l and order m of the disturbing potential, GM and a are scaling constants, and $\hat{\boldsymbol{x}} = \boldsymbol{x}/|\boldsymbol{x}|$ is the projection of the computation point

$\boldsymbol{x}$ onto the surface of the unit sphere. The ellipsoidal height of the quasi-geoid above the GRS80 ellipsoid at the point $\boldsymbol{x}$, which is referred to as the height anomaly, is

$$\zeta(\boldsymbol{x}) = \frac{T(\boldsymbol{x})}{\gamma(\boldsymbol{x}_0)} \ , \tag{2}$$

where $\gamma(\boldsymbol{x}_0)$ is the normal gravity at the telluroid point $\boldsymbol{x}_0$. In this study, we can replace the normal gravity at the telluroid by a representative constant, e.g., GM/a^2 , or simply by $\gamma \approx 9.81$ m s^{-2}. When using the first option, the height anomaly can be computed as

$$\zeta(\boldsymbol{x}) = a \sum_{l=0}^{\infty} \sum_{m=-l}^{l} \overline{c}_{lm} \left(\frac{a}{|\boldsymbol{x}|} \right)^{l+1} \overline{Y}_{lm}(\hat{\boldsymbol{x}}) \ , \tag{3}$$

where $\boldsymbol{x}$ is a point on the Earth's surface or, without introducing additional errors, on the telluroid.

The spherical harmonic coefficients in Eq. (3) can be estimated from a global terrestrial gravity data set, provided that gravity is measured at all points on the Earth's surface. In reality, gravity can only be measured at a finite number of points. When assuming a homogeneous data coverage, it makes sense to define a mean distance Δ between the gravity data points. From this data set, all coefficients complete to a maximum degree L can be estimated, where L is related to Δ as

$$L = \frac{180^\circ}{\Delta} \ , \tag{4}$$

where Δ is in units of degrees. The coefficients of degree $l > L$ are not resolved by a global data set with spacing Δ, and, therefore, are left unknown. Their contribution to the height anomaly is referred to as the height anomaly omission error

$$\zeta_{om}(\boldsymbol{x}) = a \sum_{l=L+1}^{\infty} \sum_{m=-l}^{l} \overline{c}_{lm} \left(\frac{a}{|\boldsymbol{x}|} \right)^{l+1} \overline{Y}_{lm}(\hat{\boldsymbol{x}}) \ . \tag{5}$$

Without knowledge about the coefficients of degrees $> L$, one cannot compute the omission error. It is, however, possible to estimate the global Root Mean Square (RMS) omission error. This requires only the knowledge of the power in the height anomalies as function of the degree. The power in height anomalies on the surface of a mean Earth's sphere of radius R, Ω_R, is defined as

$$P = \frac{1}{4\pi R^2} \int_{\Omega_R} \zeta^2 d\Omega_R \ . \tag{6}$$

The quantity $\sqrt{P}$ is referred to as the RMS height anomaly. Using the orthogonality properties of surface spherical harmonics, it is straightforward to show that

$$P = \sum_{l=0}^{\infty} \sigma_{l,R}^2 \ , \tag{7}$$

with

$$\sigma_{l,R}^2 = a^2 \left(\frac{a}{R} \right)^{2l+2} \sum_{m=-l}^{l} \bar{c}_{lm}^2 \ . \tag{8}$$

For a fixed degree l, $\sigma_{l,R}^2$ is the contribution to the power in height anomalies of the $2l + 1$ coefficients of degree l. They are referred to as height anomaly degree variances at the surface of a sphere of radius R. When summing up the contributions to the power of all degrees > L, we obtain the power of the height anomaly omission error on the surface of a sphere of radius R

$$P_{om} = \frac{1}{4\pi R^2} \int_{\Omega_R} \zeta_{om}^2 \, d\Omega_R = \sum_{l=L+1}^{\infty} \sigma_{l,R}^2 \ , \tag{9}$$

in which, the quantity $\sigma_{om} = \sqrt{P_{om}}$ is referred to as the global RMS omission error. To compute P_{om}, one needs to know the height anomaly degree variances for degrees > L. They are unknown as are the coefficients of degrees > L. However, it is known from an analysis of global gravity data that the height anomaly power spectrum approximately follows a power law, i.e., the height anomaly degree variances are of the order $O\left(l^{\alpha}\right)$ for some $\alpha < -1$. This knowledge is used to estimate height anomaly degree variances even at degrees for which no data are available (i.e., for degrees > L). First, from available global gravity data, the height anomaly degree variances are computed for all degrees $\leq L$, providing what is referred to as empirical height anomaly degree variances. Then, an analytical function is fitted to them by least-squares. Height anomaly degree variances for degrees > L are then obtained by extrapolation. Based on such fits, expressions for the global RMS height anomaly omission error have been derived in the past by several authors. Examples are (*Kaula, 1966*)

$$\sigma_{om} = 10^{-5} R \sqrt{\sum_{L+1}^{\infty} \frac{2l+1}{l^4}} \approx \frac{64}{L} \ \ [\text{m}] \ , \tag{10}$$

and (*Jekeli, 2012*)

$$\sigma_{om} = \frac{2043}{L^{1.653}} \ \ [\text{m}] \ . \tag{11}$$

Numbers obtained in this way represent global mean estimates of the omission error. The omission error in a particular region may differ from this global mean. The reason is that topography and bathymetry are the dominant contributors to the height anomaly

degree variances at relatively high degrees (*Turcotte, 1987*). Hence, the differences with respect to the global mean will be the largest in regions that are either much more flat or rough than the Earth is on average. In the former case, the global mean overestimates the omission error, whereas in the latter case it underestimates this error. *Jekeli (2012)* studied several areas in the US with different topographic characteristics. He found the model

$$\sigma_{om} = \frac{2567}{L^{1.717}} \text{ [m]} \tag{12}$$

for a flat area, and the model

$$\sigma_{om} = \frac{2883}{L^{1.537}} \text{ [m]} \tag{13}$$

for a mountainous area with the Rocky mountains in the north. The main difference between Eqs (12) and (13) is in the exponent of L, which decreases from 1.717 for the flat area to 1.537 for the mountainous one. A smaller exponent means that there is relatively more power in the higher degrees, and this is caused by the strong topography in the mountainous area. Figure 1 shows the omission errors as described by Eqs (11)–(13) as function of the mean distance between the data points. This distance, which is related to L as $\pi R/L$, is referred to as data spacing or half wavelength data resolution. Figure 1 shows that for the rough area in the US, one needs at least one data point per 2 km to keep the omission error below 2.5 mm, cf. Eq. (13). Over the flat area in the US, the data spacing can be larger, about 6 km, cf. Eq. (12). When using the global omission error model, Eq. (11), a data spacing of about 5 km is required. This means that the global model underestimates the omission error in the rough area significantly, e.g., by a factor of about

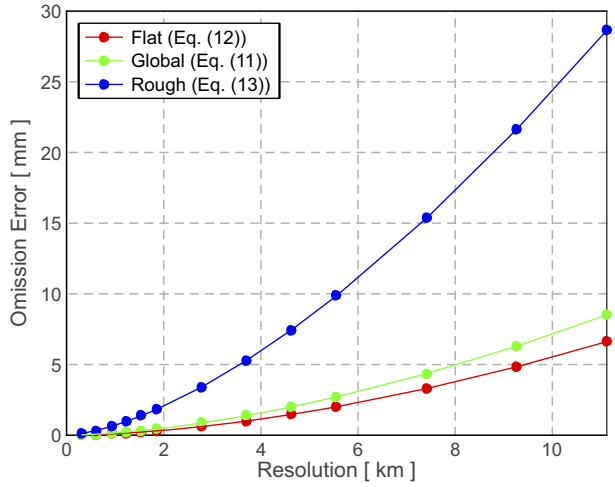

Fig. 1. The omission error as a function of the data spacing. All models are taken from *Jekeli (2012)*.

four for a data point distance of 8 km. This is the primary reason why regional studies need to be performed for areas with a topography significantly different from the global mean topography. Another reason are regional mass density anomalies, which may have a significant impact on the height anomaly degree variances at regional scales (e.g., *Sjöberg, 2004*).

2.2. Methodology

It is known that the very short wavelengths of the Earth's gravity field are mainly determined by the Earth's topography, including bathymetry (e.g., *Hirt et al., 2013*). Today, models of the land topography are known with much higher spatial resolution than any gravity data set. In ocean areas, the situation is less favorable though the spatial resolution of bathymetric models still exceeds that of marine gravity data. Therefore, surface gravity data sets, which are limited in terms of spatial resolution, are complemented with topography-induced gravity data sets, which are of a much higher spatial resolution. This yields a gravity data set with the spatial resolution of the topography-induced gravity data, which could serve as a reference for the computation of the height anomaly omission error. Such an ultra-high resolution data set was produced and exploited by *Jekeli et al., (2009)* and *Jekeli (2012)* to yield the height anomaly omission error models, Eqs (12) and (13). Basically, the same approach is followed in this manuscript. Thus, we provide a summary of the main steps and equations used in this study. For more details, we refer to *Jekeli et al., (2009)* and *Jekeli (2012)*.

The overall approach followed in this manuscript to compute the height anomaly omission error comprises a number of steps. It begins with the production of an ultra-high resolution gravity anomaly data set. The gravitational potential of topography and bathymetry is computed using Airy's isostatic model and Helmert's condensation method with a compensation depth of $D = 30$ km. When assuming a constant mass density of the crust and of the ocean water, the topography-implied gravitational potential is (*Heiskanen and Moritz, 1967*)

$$V(\boldsymbol{x}) = GR^2\rho\iint_{\sigma}\frac{h(\boldsymbol{y})}{|\boldsymbol{x}-\boldsymbol{y}|}\,d\sigma(\boldsymbol{y}) - G(R-D)^2\,\rho\iint_{\sigma}\frac{h(\boldsymbol{y})}{|\boldsymbol{x}-\boldsymbol{y}|}\,d\sigma(\boldsymbol{y}), \tag{14}$$

where G is the Newton's gravitational constant and

$$h = \begin{cases} H & \text{for points on land,} \\ -\left(1-\dfrac{\rho_w}{\rho}\right)B & \text{for points on ocean.} \end{cases} \tag{15}$$

Herein, H is the height of the topography above the quasi-geoid, B is the distance between the sea floor and the quasi-geoid, ρ is the density of the Earth's crust, and ρ_w is the density of the ocean water. The topography-implied gravity anomalies are approximately equal to $-\partial V/\partial|\boldsymbol{x}|$. They are evaluated using the Fourier transform of a planar approximation to Eq. (14) (*Forsberg, 1985*)

$$\Delta g = 2\pi G\rho \mathrm{F}^{-1}\left(\mathrm{F}\left(h\right)\left(1-\mathrm{e}^{-2\pi\omega D}\right)\mathrm{e}^{-2\pi\omega z}\right) , \tag{16}$$

where F is the Fourier transform operator and z is the distance of the computation point to the quasi-geoid. To further simplify the computations, we evaluate Δg at the quasi-geoid by setting $z = 0$ for all evaluation points. Taking into account that the topography h is given typically on a regular $I \times J$ grid with widths Δx and Δy, respectively, we evaluate the topography-implied gravity anomalies using the 2D Discrete Fourier transform (DFT)

$$\Delta g_{ij} = 2\pi G\rho\left\{\mathrm{DFT}^{-1}\left(\mathrm{DFT}\left(h\right)_{nm}\left(1-\mathrm{e}^{-2\pi\omega_{nm}D}\right)\right)\right\}_{ij} , \tag{17}$$

with

$$\omega_{ij} = \sqrt{\mu_i^2 + \upsilon_j^2} , \tag{18}$$

$$\mu_i = \begin{cases} \dfrac{i}{I\Delta x} & \text{for } i = 0, \ldots, \dfrac{I}{2}-1 , \\ \dfrac{i-I}{I\Delta x} & \text{for } i = \dfrac{I}{2}, \ldots, I-1 , \end{cases} \tag{19}$$

$$\upsilon_i = \begin{cases} \dfrac{j}{J\Delta y} & \text{for } j = 0, \ldots, \dfrac{J}{2}-1 , \\ \dfrac{j-J}{J\Delta y} & \text{for } j = \dfrac{J}{2}, \ldots, J-1 , \end{cases} \tag{20}$$

i and $n = 0, \ldots, I-1$ and j and $m = 0, \ldots, J-1$.

To make the topography-implied gravity anomalies consistent with the available (i.e., measured) surface gravity anomalies, we triangulate the latter ones using the Delaunay triangulation. Within each triangle, a plane is fitted by least-squares through the topography-implied gravity anomalies. Next, the planar model is subtracted from the topography-implied gravity anomalies, giving reduced topography-implied gravity anomalies. Finally, a planar model that is fitted to the measured gravity anomalies at the corners of each triangle is added to the reduced topography-implied gravity anomalies, providing the final high-resolution gravity anomaly data set, to which we refer as "topography-implied and measurement-adjusted gravity anomalies".

The high-resolution gravity anomaly data set from the previous step is reduced for the contribution of a global gravity model (GGM), providing a high-resolution residual gravity anomaly data set, denoted as $\delta\Delta g$. This data set is referred to as the "reference gravity anomaly data set". From this data set, residual height anomalies, $\delta\zeta$, are computed using a planar approximation of the Stokes integral (*Heiskanen and Moritz, 1967*)

$$\delta\zeta_i = \delta\zeta\left(\boldsymbol{x}_i\right) = \frac{1}{2\pi\gamma}\iint\limits_{\Omega_i}\frac{\delta\Delta g\left(\boldsymbol{y}\right)}{\left|\boldsymbol{x}_i - \boldsymbol{y}\right|}\, d\Omega_i\left(\boldsymbol{y}\right) , \tag{21}$$

where $\gamma = 9.81$ m s^{-2} is a mean value of the gravity and Ω_i is the integration domain for the evaluation point $\boldsymbol{x}_i$. The residual height anomalies computed in this way, which are referred to as "reference height anomalies", represent the reference values with respect to which omission errors are quantified. It is worth noting that they also suffer from an omission error. However, this error is extremely small seen the ultra high spatial resolution of the "reference gravity anomalies" used in their computation, and, therefore, can be neglected.

Given the "reference gravity anomalies", lower-resolution gravity anomaly data sets are generated by sub-sampling the "reference gravity anomalies"'. For each of the sub-sampled gravity anomaly data set, residual height anomalies are computed, and the differences with respect to the "reference height anomalies" are interpreted as omission error of the corresponding sub-sampled gravity anomaly data set. The RMS difference is taken as a measure of the omission error.

2.3. Practical aspects

In this study, we make use of a blend of the $2'' \times 2''$ European DEM, EuroDEM (*EuroGeographics, 2008*), $1'' \times 1''$ Shuttle Radar Topography Mission, SRTM (*Farr et al., 2007*), and $30'' \times 30''$ General Bathymetric Chart of the Oceans, GEBCO (*Gebco Gridded Global Bathymetry Data, British Oceanographic Data Centre, www.bodc.ac.uk*). From them, we generate a homogeneous $2'' \times 2''$ DEM using the cubic spline interpolation. This $2'' \times 2''$ DEM is used when computing the topography-implied high-resolution gravity anomaly data set.

The measured surface gravity anomalies are taken from the gravity database used in *Slobbe and Klees (2014)* and *Slobbe et al., (2014)*. The high-resolution gravity anomaly data set, which is a blend of the measured surface and topography-implied gravity anomaly data sets, are computed on a $2'' \times 2''$ grid. Figure 2 shows the measured surface gravity anomalies and the $2'' \times 2''$ high-resolution gravity anomalies for two $3° \times 3°$ areas in the Netherlands.

This grid size, which corresponds to about 38 m at the latitude of 50°, is substantially smaller than the half wavelength resolution of the measured surface gravity anomalies, which is about 2 km on land and 30 km at sea, when considering only shipboard gravity anomalies.

The evaluation of Eq. (21) at many points is a time-consuming operation. We control the numerical effort in three ways. First, we do not compute height anomalies for the whole Netherlands mainland and continental shelf, but limit the computations to two $1° \times 1°$ test areas. Since the omission error is controlled by topography, with larger omission errors in rough terrain and vice versa, one test area has a flat topography, whereas the other is characterized by a rougher terrain. The topography and bathymetry over the two selected areas are shown in Fig. 3. The selected flat test area is located in the central part of the Netherlands and is almost flat. The selected rougher test area is located in eastern Belgium, south of the border to the Netherlands. This area is dominated by the mountain range of the Ardennes with variations in elevations of more than 800 m.

Second, to compute the "reference gravity anomalies", we reduce the high-resolution "topography-implied and measurement-adjusted gravity anomalies" for the contribution of the regularized version of GOCO05S (*Pail et al., 2010*; *Mayer-Gürr et al., 2015*) complete to degree 280. This allows the limitation of the integration domain Ω_i of

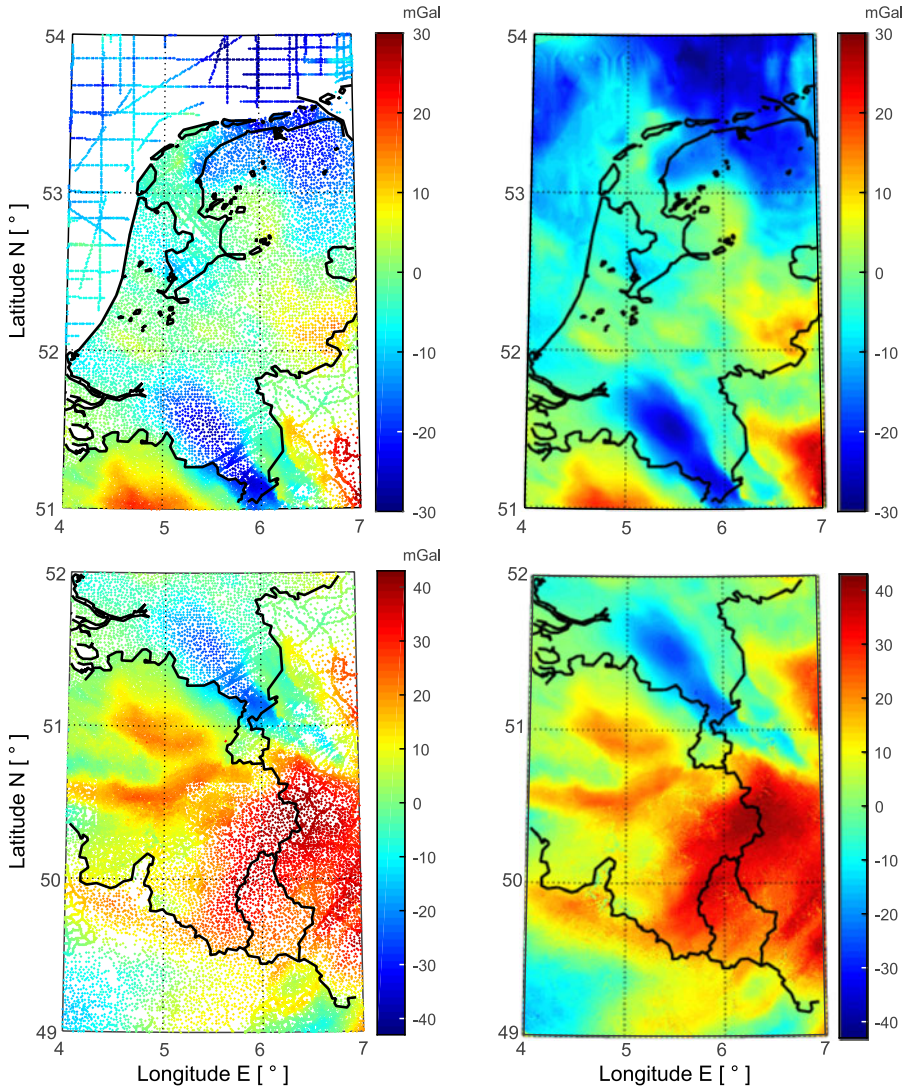

Fig. 2. Gravity anomalies in two 3° × 3° areas in the Netherlands: the measured surface gravity anomalies (left) and the 2″ × 2″ "topography-implied and measurement-adjusted gravity anomalies" (right). The selected flat and rough 1° × 1° test areas are located at the centre of the areas shown in the top and bottom rows, respectively.

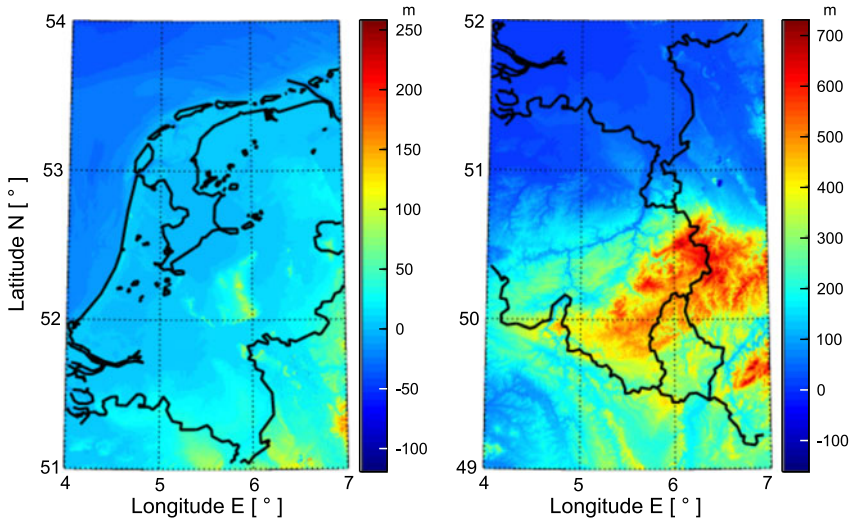

Fig. 3. Topography and bathymetry on a $2'' \times 2''$ grid over two selected $3° \times 3°$ areas in the Netherlands. The $1° \times 1°$ test areas are located at the centre of the areas shown in the plots. The test area shown in the left panel is flat with little topography or bathymetry, whereas the one shown in the right panel is characterized by a rougher terrain, particularly in the south-eastern part with mountains up to 800 m.

Eq. (21) to a neighborhood of the computation point $\boldsymbol{x}_i$. This integration domain comprises the areas shown in Fig. 2 for the selected flat test area (top panel) and the selected mountainous area (bottom panel), no matter where the computation point $\boldsymbol{x}_i$ is located. This ensures that all gravity data within a distance of at least 1° around the computation point are incorporated in the evaluation of Eq. (21). This distance is sufficiently large since it is larger than the half wavelength spatial resolution of GOCO05S, i.e., $180^\circ/280 \approx 0.6^\circ$, cf. Eq. (4).

Third, Eq. (21) is evaluated using numerical integration. Since the "reference gravity anomalies" used in this study are produced as gridded data in an image domain with Cartesian coordinates (x, y), we use a simple composed Newton-Cotes cubature formula (*Jekeli et al., 2009*)

$$\delta\zeta_{ij} = \sqrt{\frac{\Delta x \Delta y}{\pi}}\frac{\delta\Delta g_{ij}}{\gamma} + \frac{\Delta x \Delta y}{2\pi\gamma}\sum_{n=0}^{I-1}\sum_{m=0}^{J-1} u_{ijnm}\delta\Delta g_{nm}\,, \tag{22}$$

where

$$u_{ijnm} = \begin{cases} 0 & i = n \text{ and } j = m\,, \\ \dfrac{1}{\sqrt{(i-n)\Delta x^2 + (j-m)\Delta y^2}} & i \neq n \text{ or } j \neq m\,, \end{cases} \tag{23}$$

Δx and Δy are the grid size in x- and y-coordinate, respectively, $i = 0, \ldots, I-1$ and $j = 0, \ldots, J-1$. Numerical tests (not shown) have demonstrated that the numerical integration error is no larger than a few percents of the omission error, and therefore, negligible.

2.4. Results

Figure 4 shows the height anomaly omission error as a function of the data spacing for the two selected 1° × 1° target areas. For the flat area, the omission error is rather small; it barely reaches 0.5 mm at a data spacing of 2 km. It is worth noting that the analytical models of *Jekeli (2012)* given in Eq. (11) (i.e. a global model) and Eq. (12) (i.e. a model computed for a flat area in the US) provide significantly larger errors above a half wavelength resolution of 6 km than those computed for the flat test area in the Netherlands (compare Fig. 1 with Fig. 4). At smaller half wavelengths, the differences are rather small.

To obtain an easily accessible description of the omission error, we fit a linear polynomial function to the curves shown in Fig. 4. For the flat test area, which is representative to the Central and Northern Netherlands and the Netherlands continental shelf, the model is

$$\varepsilon_{om}\,[\mathrm{mm}] = 0.32d\ , \tag{24}$$

where d is the data spacing in units of kilometres. For the hilly test area, which is representative to the Southern Netherlands, the linear omission error model is

$$\varepsilon_{om}\,[\mathrm{mm}] = 0.92d\ . \tag{25}$$

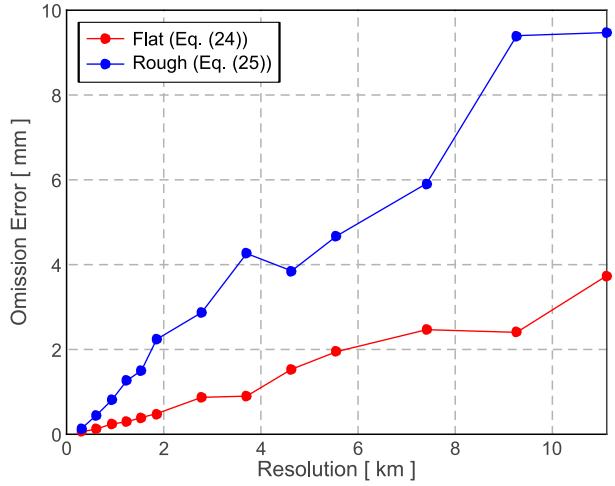

Fig. 4. Height anomaly omission error computed for the two selected 1° × 1° test areas (cf. Fig. 3) as function of the data spacing.

3. COMMISSION ERROR

3.1. Methodology

The height anomaly commission error is the contribution of errors in gravity data to the height anomalies. Here, we assume that errors in gravity data are zero-mean white Gaussian and homogeneous, which is a common assumption in commission error analysis studies (e.g., *Jekeli et al., 2009*). Then, the data noise is uniquely described by the noise standard deviation. From a measurement process point of view, the white noise assumption is justified. In reality, however, the situation is worse as many surface gravity data sets suffer from long-wavelength systematic errors (*Heck, 1990*). Some of these errors are caused by unknown height system offsets. They introduce systematic errors in normal gravity values, which in turn, map one-to-one into gravity anomalies. Their impact on a computed quasi-geoid model may be mitigated by co-estimating bias parameters per surface gravity data set. This approach is followed in, e.g., *Slobbe (2013)* and *Slobbe and Klees (2014)*.

The commission error depends on the methodology used to estimate the (quasi-) geoid. Several methods are used in practice, among others, methods based on the Stokes integral or Stokes-type integrals (e.g., *Jekeli, 1981*; *Vaníček et al., 1999*; *Novák et al., 2001*; *Sjöberg, 2003*), least-squares collocation (*Moritz, 1978*; *Tscherning, 1978, 1985*), and least-squares techniques (e.g., *Eicker, 2008*; *Klees et al., 2007, 2008*; *Schmidt et al., 2007*; *Wittwer, 2009*). Each method deals with the data noise in a different way, hence, they may lead to different estimations of the commission error. In this study, we use the Stokes integral (e.g., *Heiskanen and Moritz, 1967*)

$$\zeta(\boldsymbol{x}) = \frac{R}{4\pi\gamma} \iint_{\Omega} S(\boldsymbol{x}-\boldsymbol{y})\,\Delta g(\boldsymbol{y})\,d\Omega(\boldsymbol{y}) \;, \tag{26}$$

where R is the radius of the mean Earth sphere, $S(\boldsymbol{x})$ denotes the Stokes kernel at the computation point $\boldsymbol{x}$, and Ω is the unit sphere. Equation (26) was used in *de Min (1996)* to compute a quasi-geoid model for the Netherlands mainland.

For the estimation of the commission error, a number of simplifications are justified. First of all, it does not matter whether Eq. (26) is interpreted in the framework of Stokes theory of the geoid or in the framework of Molodensky's theory of the quasi-geoid. In this study, we call ζ the height anomaly, i.e., we work in the framework of Molodensky's theory, and ζ is the ellipsoidal height of the quasi-geoid above the GRS80 reference ellipsoid. Then, Eq. (26) is a zero-order approximation of the height anomaly. This, together with $\gamma = 9.81$ m s^{-2}, is sufficiently accurate for the commission error analysis.

Furthermore, common to the application of Eq. (26) is that Δg does not contain the contribution of a GGM, i.e., it is in fact a residual quantity. Likewise, ζ in Eq. (26) is the residual height anomaly. Then, the integration is not performed over the whole unit sphere Ω, but only over a spherical cap centred at the computation point $\boldsymbol{x}$, $\Omega_c(\boldsymbol{x})$. The diameter of the spherical cap depends, among others, on the maximum degree of the GGM. There is no simple rule that provides the diameter of the spherical cap given the

maximum degree of the GGM. The only statement that can be made is that the diameter must not be smaller than the half wavelength spatial resolution of the GGM.

Another aspect to be considered is that, in practice, the Stokes kernel S in Eq. (26) is replaced by a modified kernel, $\tilde{S}$. Originally, kernel modifications were introduced to reduce the truncation error, which is caused by limiting the integration to the spherical cap $\Omega_c(\boldsymbol{x})$. Later, so-called stochastic kernel modifications were suggested, which aim at minimizing a combination of various errors or the total mean square error. For the computation of the height anomaly commission error caused by errors in the surface gravity anomalies, as considered here, a deterministic modification of the Stokes kernel is to be preferred. Here, we use the spheroidal Stokes kernel (*Vaníček and Kleusberg, 1987*), which reads as

$$\tilde{S}(\boldsymbol{x}-\boldsymbol{y}) = S(\boldsymbol{x}-\boldsymbol{y}) - \sum_{l=2}^{L} \frac{2l+1}{l-1} P_l\left(\hat{\boldsymbol{x}}^{\mathrm{T}}\hat{\boldsymbol{y}}\right) . \tag{27}$$

Herein, $\hat{\boldsymbol{x}}$ and $\hat{\boldsymbol{y}}$ are the projections of $\boldsymbol{x}$ and $\boldsymbol{y}$, respectively, on the surface of the unit sphere, P_l denotes the Legendre polynomial of degree l, and L is the maximum degree of the GGM used in the remove-compute-restore approach to the Stokes integral. Note that the commission error depends on the type of kernel modification as does the truncation error. As the latter is not considered as a part of the commission error, the commission error for a particular kernel modification has to be interpreted with care. To get an idea about the impact of a kernel modification on the commission error, we also compute the commission error for the spherical Stokes kernel.

There are different techniques of how to evaluate an integral like that of Eq. (26). The reason is that the residual gravity anomalies are not available at any point on the surface, but only at the data locations. When using just this information and not relying upon any type of spatial interpolation, a simple discretization of Eq. (26) reads as

$$\zeta(\boldsymbol{x}) \approx \frac{R}{4\pi\gamma} \frac{|\Omega_c|}{I} \sum_{i=1}^{I} S(\boldsymbol{x}-\boldsymbol{y}_i)\Delta g(\boldsymbol{y}_i) , \tag{28}$$

where $\boldsymbol{y}_i$ are the data locations, $|\Omega_c|$ is the area of the spherical cap integration domain, and I is the number of data points inside the spherical cap. There is a problem with Eq. (28) when the computation point $\boldsymbol{x}$ is identical or close to any of the data points $\boldsymbol{y}_i$. Then, the Stokes kernel would go to infinity or takes up very large values, which may corrupt the commission error computation. Alternatively, one may use the planar approximation of the Stokes integral, Eq. (22), in which the weak singularity of the Stokes kernel has been isolated. In this study, we use another approach. It is based on writing Eq. (26) as an integral over the spherical polar coordinates (ψ, α) centred at the computation point $\boldsymbol{x}$. Then, $S(\boldsymbol{x}-\boldsymbol{y})$ reads as

$$S(\boldsymbol{x}-\boldsymbol{y}) = S(\psi) = \frac{1}{s} - 6s - 4 + 10s^2 - \left(3 - 6s^2\right)\ln\left(s + s^2\right) , \tag{29}$$

where $s = \sin(\psi/2)$, ψ is the spherical distance between the computation and integration points, and α is the spherical azimuth between those points (*de Min, 1996*). With $d\Omega(\boldsymbol{y}) = \sin\psi \; d\psi \; d\alpha$, we can rewrite Eq. (26) as

$$\zeta(\boldsymbol{x}) = \frac{R}{4\pi\gamma} \int_0^{2\pi} \int_0^{\psi_c} K(\psi) \Delta g(\psi, \alpha) \, \mathrm{d}\psi \, \mathrm{d}\alpha \;, \tag{30}$$

where ψ_c is the radius of the spherical cap, and

$$K(\psi) = S(\psi) \sin\psi \tag{31}$$

$$= 2\cos\frac{\psi}{2} - \left[6s + 4 - 10s^2 + \left(3 - 6s^2\right) \ln\left(s + s^2\right) \right] \sin\psi \;. \tag{32}$$

$K(\psi)$ does not have any singularity. Again, when we only rely upon the given gravity anomaly data set (i.e., no spatial interpolation), a simple discretization of Eq. (30) reads as

$$\zeta(\boldsymbol{x}) = \frac{R\psi_c}{2\gamma I} \sum_{i=1}^{I} K(\psi_i) \Delta g(\psi_i, \alpha_i) \;. \tag{33}$$

Equation (33) has to be preferred upon Eq. (28) as the kernel K is smooth for all spherical distances. Using Eq. (33) to compute the commission error, however, gives an estimate which also contains the integration error, i.e., the difference between Eqs (30) and (33). If one wishes to eliminate the integration error, one needs to use more powerful numerical integration formulas such as Gauss-Legendre formulas. Their application requires data interpolation to the nodes of the Gauss-Legendre formulas. Suppose that $\{\psi_i, w_i\}$ are the nodes and weights of an I-point Gauss-Legendre quadrature formula over $[0, \psi_c]$, and $\{\alpha_j, v_j\}$ are the nodes and weights of a J-point Gauss-Legendre quadrature over $[0, 2\pi]$. Then, the discretization of Eq. (30) reads as

$$\zeta(\boldsymbol{x}) = \frac{R}{4\pi\gamma} \sum_{i=1}^{I} \sum_{j=1}^{J} w_i v_j K(\psi_i) \Delta g(\psi_i, \alpha_j) \;, \tag{34}$$

where the total number of nodes is $I\,J$. Given the data resolution Δ in radians and ψ_c in radians, logical choices for I and J would respectively be

$$I = \frac{\psi_c}{\Delta} \tag{35}$$

and

$$J = \frac{2\pi}{\Delta} \;. \tag{36}$$

What makes this approach critical is that J will be unrealistically large. For instance, if the data spacing is 1 km and the radius of the spherical cap is 5°, then $I = 556$ and $J = 4 \times 10^4$, i.e., $IJ = 2.2 \times 10^7$. Compared to this number, a rectangle of side length of 10° contains only about 10^6 data points. Therefore, we use the following approach to fix I and J. The goal is to find a number of nodes that is comparable to the number of data points inside the spherical cap for a given data resolution. Suppose that the data spacing is Δ in radians and the radius of the spherical cap is ψ_c in radians. Then, there are about $\left(2\psi_c/\Delta\right)^2$ data points inside a rectangle enclosing the spherical cap. Hence, we force IJ to be equal to this number. With

$$I = \frac{\psi_c}{\Delta} \ , \tag{37}$$

which is a natural choice for the number of nodes in ψ, we obtain

$$J = \frac{4\psi_c}{\Delta} \ . \tag{38}$$

In this study, we use the discretization of Eq. (34) with the choice given in Eqs (37) and (38) to evaluate the commission error. Switching to errors, Eq. (34) reads as

$$\varepsilon_\zeta = \frac{R}{4\pi\gamma} \sum_{i=1}^{I} \sum_{j=1}^{J} w_i v_j K\left(\psi_i\right) \varepsilon_{\Delta g}\left(\psi_i, \alpha_j\right) \ . \tag{39}$$

Assuming zero mean white Gaussian noise with a standard deviation $\sigma_{\Delta g}$, the noise standard deviation of residual height anomalies ζ is

$$\sigma_\zeta = \sigma_{\Delta g} \frac{R}{4\pi\gamma} \sqrt{\sum_{j=1}^{J} v_j^2 \sum_{i=1}^{I} \left(w_i K_i\right)^2} \ , \tag{40}$$

with $K_i = K\left(\psi_i\right)$. Equation (40) is used in this study to compute the height anomaly commission error due to errors in terrestrial gravity anomalies. Notice that it does not depend on the location of the computation point as the spherical distances ψ_i are the same for every computation point.

For the computation of the commission error when using the spheroidal Stokes kernel, we simply replace K in Eq. (40) with $\tilde{K} := \tilde{S} \sin\psi$, where $\tilde{S}$ is taken from Eq. (27).

3.2. Results

To compute the commission error in case of the spheroidal Stokes kernel, we set L in Eq. (27) to 100. The reason for this choice is provided later when we discuss the commission error of the GGM. Figure 5 shows the height anomaly commission error as a function of the data spacing assuming a zero-mean white Gaussian noise of 1 mGal standard deviation in surface gravity anomalies. For noise standard deviations different

from 1 mGal, the commission error can easily be computed as it scales linearly with the noise standard deviation according to Eq. (40). Figure 5 shows that the commission error depends on the radius of the spherical cap. For the spherical Stokes kernel, this dependency is negligible for cap radii below, say, 10° and a data resolution of better than, say, 10 km. For the spheroidal Stokes kernel, the impact of the cap radius on the commission error is larger. Figure 5 also reveals that when using the spheroidal Stokes kernel, the commission error does not increase monotonously with increasing cap radius as it does when using the spherical Stokes kernel. Depending on the size of the data area, this might be used to further reduce the commission error by fine-tuning the radius of the spherical cap. Finally, we see that using the spheroidal Stokes kernel reduces the commission error by a factor of 2.2 compared to the use of the spherical Stokes kernel. The dashed curve in Fig. 5, showing the largest errors, refers to an integration domain that is equal to the whole sphere. Hence, it refers to the case that no GGM is used, and the height anomalies are computed using a global gravity anomaly data set. Though this does not correspond to the current practice in regional (quasi-) geoid modelling, it gives insight into the role of the GGM in quasi-geoid modelling. Without using a GGM, the data requirements are pretty stringent. A commission error of 2.5 mm requires a global coverage with surface gravity anomaly data of 1 mGal standard deviation and 1.5 km data spacing. When doubling the data noise standard deviation to 2 mGal, the required data spacing is about 0.7 km. Neither is feasible today.

This is one of the reasons why the use of a GGM is indispensable in regional quasi-geoid determination. The main implication of using a GGM, however, is that the commission error comprises two components: (i) the commission error due to errors in the surface gravity anomalies, and (ii) the commission error due to errors in the GGM. What the real commission error is when using a GGM in combination with surface gravity

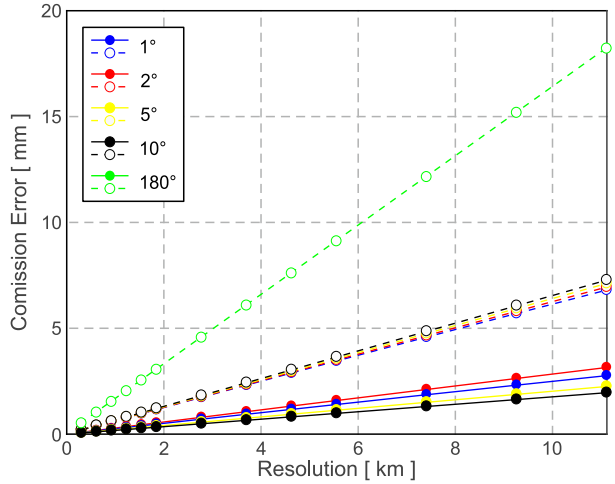

Fig. 5. Height anomaly commission error as a function of the data resolution for zero-mean white Gaussian noise of 1 mGal standard deviation in surface gravity anomalies when using the spherical Stokes integral (dashed lines) and the spheroidal Stokes integral (solid lines). Lines need to be scaled by x if the data noise standard deviation is x mGal.

anomalies depends on the methodology of data combination. Methods using Stokes-type integrals exploit stochastic kernel modifications or a combination of stochastic and deterministic kernel modifications to minimize the sum of several error sources or the total mean square error. In least-squares techniques or least-squares collocation, the GGM may be considered as another noisy data set like the surface gravity anomaly data set, which implies that it directly contributes to the commission error. Here, we follow a more simplistic approach and compute the commission error as

$$\sigma_{com} = \sqrt{\sigma_{\mathrm{GGM}}^2 + \sigma_\zeta^2} \ , \tag{41}$$

where σ_{GGM} is the commission error of the GGM and σ_ζ is the commission error of surface gravity anomaly data. We expect that Eq. (41) provides an upper bound of the real commission error.

To obtain an estimate of the commission error of the GGM, we use the full noise covariance matrix of the un-regularized GOCO05S model (*Mayer-Gürr et al., 2015*). The full noise covariance matrix of the spherical harmonic coefficients is propagated into height anomalies. Figure 6 shows a spatial rendition of the height anomaly noise standard deviations of this model for the area 49°–63°N and 6°W –10°E. The noise standard deviation is not homogeneous. It varies between 1.1 cm and 1.8 cm with larger values in the southern part of the area and smaller values at higher latitudes. Figure 7 shows the commission error of the GOCO05S model evaluated along a parallel circle at a latitude of about 50° in Southern Netherlands. We see that the GGM commission error increases logarithmically with the truncation degree. It is well modelled by the function

$$\sigma_{\mathrm{GGM}}\,[\mathrm{m}] = \exp\left(0.03676L - 11.419\right) , \tag{42}$$

where L is the maximum degree up to which GOCO05S is used with $L \le 280$. Using GOCO05S complete to degree 200 implies a mean GGM commission error of about 1.5 cm. This is too large for the realization of a 5-mm quasi-geoid. Hence, we need to limit the use of this GGM to a maximum degree much lower than 200. For instance, when using GOCO05S only up to degree 100, the commission error is about 0.5 mm. This is negligible compared to the commission error of the surface gravity anomaly data set (cf. Fig. 5). Using this model only up to degree 100 requires a spherical cap radius of larger than 0.9°. This does not impose a limitation on the computation of the Netherlands quasi-geoid, as access to surface gravity anomalies within a few degrees outside the border of the country is granted. Hence, by limiting the maximum degree of the GGM, we can make the contribution of the GGM to the commission error negligibly small compared to the contribution of the surface gravity anomaly data set. Note that this requires a proper application of residual terrain modeling (e.g., *Forsberg, 1984*).

From now on, we neglect the commission error of the GGM. Then, Fig. 5 reveals that the commission error is well described by a linear function of data spacing, scaled by the data noise standard deviation. A least-squares fit to the curve in Fig. 5 associated with the 2° spherical cap radius provides the following simple models for the commission error

$$\sigma_{com}\,[\mathrm{mm}] = \begin{cases} 0.610\, d\, \sigma_{\Delta g} & \text{spherical Stokes kernel}, \\ 0.277\, d\, \sigma_{\Delta g} & \text{spheroidal Stokes kernel}, \end{cases} \tag{43}$$

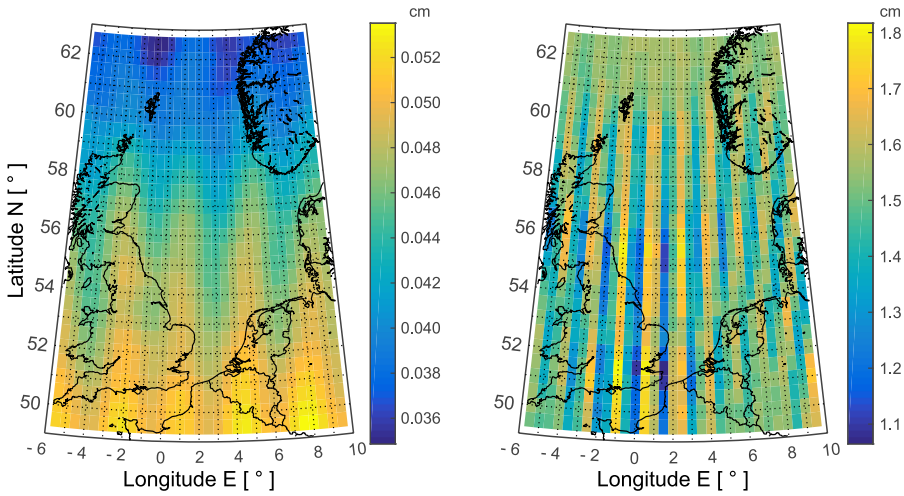

Fig. 6. Spatial rendition of the height anomaly noise standard deviation propagated from the unregularized full noise covariance matrix of GOCO05S complete to degree 100 (left) and 200 (right).

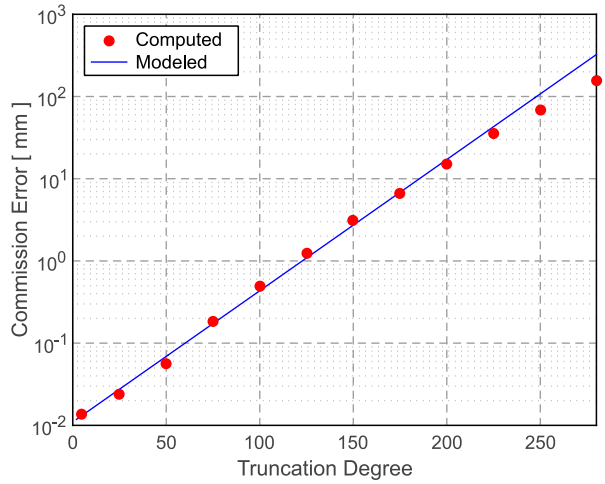

Fig. 7. Commission error of height anomalies (dots) for the global gravity field model GOCO05S as function of the truncation degree, computed along the southern border of the Netherlands (about 50°N latitude). For this latitude and geographic location, it can be well described by Eq. (42) (line).

where d is the data spacing in kilometres and $\sigma_{\Delta g}$ is the surface gravity anomaly noise standard deviation in mGal. Hence, assuming that the gravity anomaly noise standard deviation is 1 mGal, a commission error of 2.5 mm requires a data spacing of 4 km and 9 km in the cases of spherical and spheroidal Stokes kernels, respectively. The data

spacing halves if the data noise standard deviation doubles. Equation (43) is used in Section 4 when analysing the total error.

4. TOTAL ERROR

The total data error comprises two components: the omission error and the commission error. The nature of these errors is different. The omission error accounts for the effect of a limited data resolution on the computed quasi-geoid. It is a deterministic error determined by the amount of power in the regional gravity field at wavelengths not resolved by the data. The commission error, on the other hand, accounts for the noise in data. Hence, it is a random error, when assuming that the data noise is random as done in this study. This error is conceptually a function of the data noise standard deviation and the data spacing.

Seen the different nature of the two error components, one has to agree upon how to define the total error. The current approach is to distribute the error budget evenly over omission and commission errors (*Jekeli et al., 2009*). That is, if the aim is to realize a 5-mm quasi-geoid, one assigns 50% of the total error budget to the (deterministic) omission error and 50% to the (random) commission error, where the latter is usually expressed in terms of the commission error standard deviation. When doing so, we may end up with two different recommendations for the data resolution, one being linked to the omission error and the other linked to the commission error. Here, we wish to avoid such an ambiguity and define the total error as the sum of omission and commission errors where the latter is expressed in terms of the data noise standard deviation. Hence, the confidence level of the total error is 68%. Alternatively, one may use another confidence interval for the commission error, for instance 95%. When adding to it the omission error, the total error may then be interpreted at the 95% confidence interval. Then, the target accuracy of the quasi-geoid model should also be interpreted as being at the 95% confidence level.

Figure 8 shows the sum of the omission error and the commission error standard deviation. As the omission error depends on the topography and bathymetry, the sum is evaluated for the flat and the rough test areas, respectively. Moreover, as the commission error scales linearly with the data noise standard deviation, we show different error curves depending on the noise level in surface gravity anomaly data. For the flat test area, a 5-mm quasi-geoid (at the confidence level 68%) is feasible with a data spacing of about 5 km and 1 mGal data noise standard deviation. The data spacing needs to be reduced to about 3 km if the data noise standard deviation increases to 2 mGal. For the spheroidal Stokes kernel, the corresponding values are 8 km and 6 km, respectively. For the rough test area and a data noise standard deviation of 1 mGal, a 5-mm quasi-geoid requires a data spacing of about 3 km (Stokes kernel) and 4 km (spheroidal Stokes kernel). This needs to be reduced to about 2 km (Stokes kernel) and 3.5 km (spheroidal Stokes kernel) if the data noise standard deviation increases to 2 mGal.

Using the empirical models (24), (25) and (43), we obtain the following models of the total data error

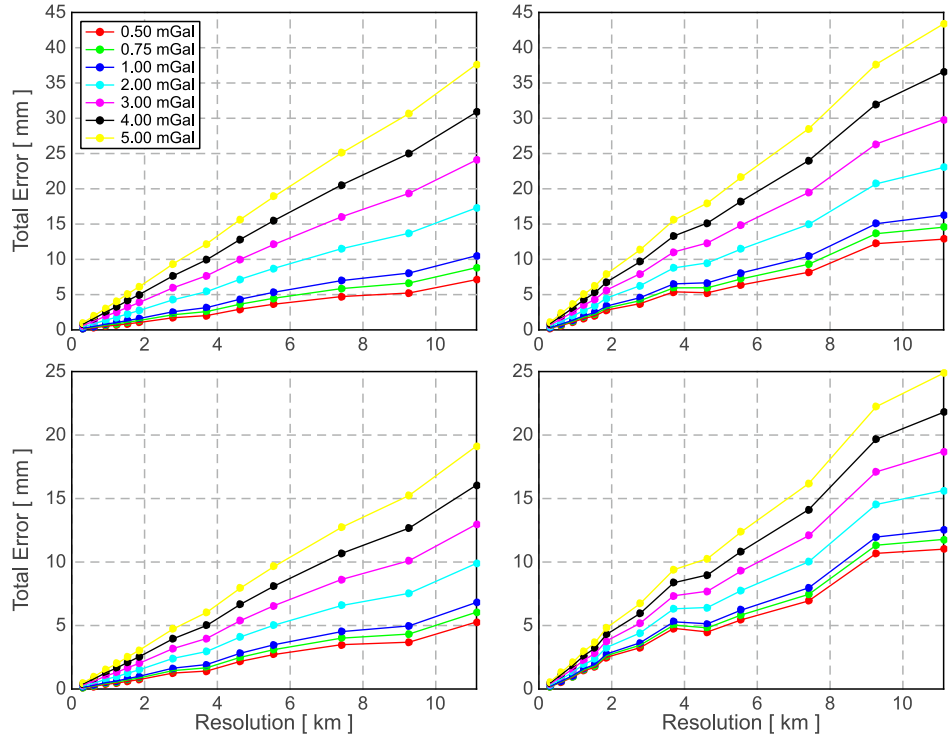

Fig. 8. Sum of commission and omission errors for the selected flat target area (top) and the rough target area (bottom) over the Netherlands for different noise standard deviations of the surface gravity anomaly data. The Stokes kernel (left column) and the spheroidal Stokes kernel (right column) are used when computing the commission error.

$$\sigma\,[\mathrm{mm}] = \begin{cases} d\left(0.32 + 0.610\,\sigma_{\Delta g}\right) & \text{spherical Stokes kernel}, \\ d\left(0.32 + 0.277\,\sigma_{\Delta g}\right) & \text{spheroidal Stokes kernel} \end{cases} \tag{44}$$

for the flat test area (which is representative for the Netherlands continental shelf and the Central and Northern Netherlands), and

$$\sigma\,[\mathrm{mm}] = \begin{cases} d\left(0.92 + 0.610\,\sigma_{\Delta g}\right) & \text{spherical Stokes kernel}, \\ d\left(0.92 + 0.277\,\sigma_{\Delta g}\right) & \text{spheroidal Stokes kernel} \end{cases} \tag{45}$$

for the rough test area (which applies to the Southern Netherlands). In Eqs (44) and (45), d is the data spacing in kilometres and $\sigma_{\Delta g}$ is the noise standard deviation of the surface gravity anomalies in mGal. A spatial rendition of Eqs (44) and (45) is shown in Fig. 9 for the two test areas.

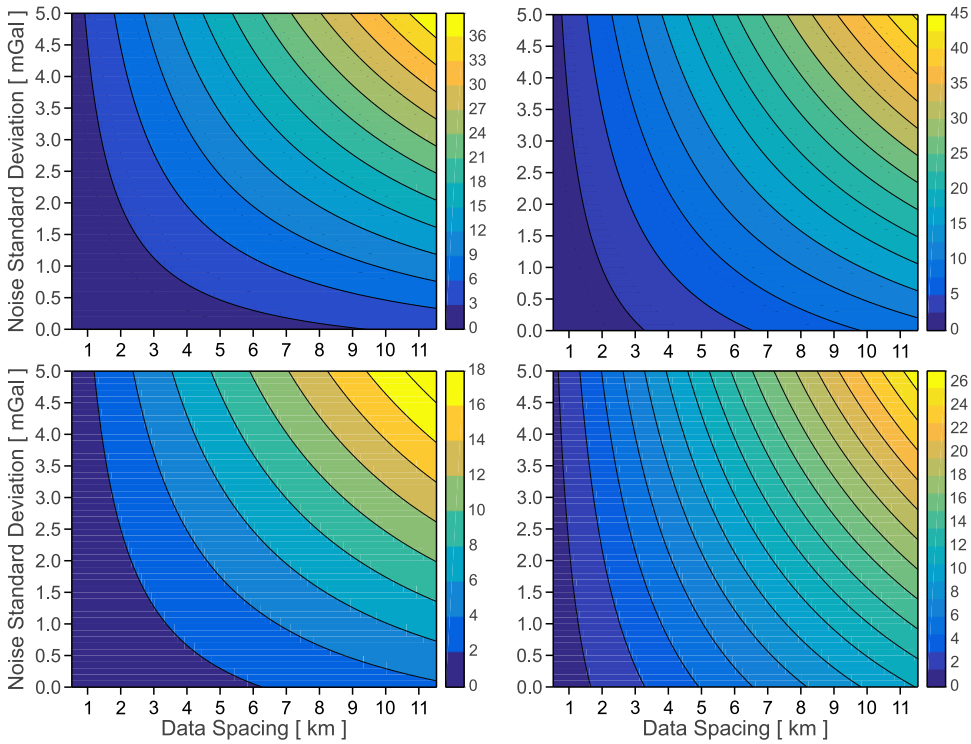

Fig. 9. Total data error in mm (at 68% confidence interval) for a selected flat terrain comparable to the North sea and the central and northern parts of the Netherlands (top row) and a selected hilly terrain comparable to the southern part of the Netherlands and the Ardennes (bottom row) as a function of data spacing in km and the gravity anomaly noise standard deviation in mGal. The Stokes kernel (left column) and the spheroidal Stokes kernel (right column) are used when computing the commission error. Note the discrete colour maps in all plots.

5. DO THE CURRENTLY AVAILABLE DATA ALLOW REALIZATION OF A 5-mm QUASI-GEOID?

The currently available data sets comprise terrestrial gravity anomalies, shipboard gravity anomalies, and radar-altimeter-based quasi-geoid height differences (e.g., *Slobbe, 2013*). They are complemented by, e.g., GOCO05S, which has a signal-to-noise ratio of one at a spherical harmonic degree of about 257. The latter corresponds to half wavelength spatial resolution of about 78 km at the equator. The discussion we provide below refers to the use of the spheroidal Stokes kernel when computing the height anomaly commission error.

The density of the terrestrial gravity anomaly data set used in the computation of the quasi-geoid for the Netherlands mainland and continental shelf is better than one point per 2 km. This is sufficient for the computation of a 5-mm quasi-geoid over the area of

interest, provided that the data noise is better than 5.7 mGal standard deviation (cf. the bottom right plot in Fig. 9). The precision estimated for the currently available terrestrial gravity anomaly data sets ranges from 0.5 mGal for the Netherlands to 2.0 mGal for Belgium. This is somewhere in between for Germany and France. Biases in the data sets can be estimated and corrected for, as is done in *Slobbe (2013)*, *Slobbe et al., (2014)*. Therefore, we may assume that the currently available continental gravity anomaly data sets are of sufficient density and quality for the realization of a 5-mm quasi-geoid model for the Netherlands mainland and continental shelf.

The situation is different for the marine area. Here, basically two data sets are available. The set of radar altimeter-based along-track quasi-geoid height differences has a spatial resolution of about one point per 7 km (*Slobbe, 2013*). The along-track mean sea surface heights have a noise standard deviation of 2–4 cm. Hence, quasi-geoid slopes have a noise standard deviation of 3–6 μrad (*Slobbe, 2013*). This corresponds to 3–6 mGal, when applying the rule-of-thumb that corresponds 1 μrad of slope to about 1 mGal of gravity anomaly (*Sandwell and Smith, 1997*; *Smith, 2010*). According to the top-right plot in Fig. 9, this causes height anomaly standard deviations of 8–14 mm, which is above the 5-mm target accuracy.

The second available data set comprises shipboard gravity anomalies. From earlier studies (e.g., *Slobbe, 2013*; *Slobbe et al., 2014*; *Farahani et al., 2017*), we know that the precision of this data set is between 1–2 mGal standard deviation. However, the point density over the Netherlands continental shelf is very inhomogeneous and there are large gaps (cf. top-left plot in Fig. 2). Along the ship tracks, the point density is extremely high. However, the gaps between the ship tracks may be as large as 30 km. The omission error has not been computed for such a coarse data resolution. An extrapolation of the empirical model of Eq. (24) yields an omission error of about 10 mm at 30 km data spacing. We expect that in reality the omission error is larger than 10 mm (cf. Fig. 4). The commission error for this data resolution is between 8–17 mm for a noise standard deviation between 1–2 mGal (cf. Fig. 5). Hence, the total data error is likely larger than 18–27 mm.

From this, we conclude that the realization of a 5-mm quasi-geoid depends critically on a better data set over the Netherlands continental shelf. It is unlikely that shipboard gravimetry is a potential candidate to fill the gap as the data acquisition is very expensive for the required spatial resolution. The coverage with radar altimeter data may improve in the future, in particular, when using high resolution data of the Sentinel mission. Assuming a future data spacing of, say, 2 km, the required accuracy in terms of gravity anomaly standard deviations needs to be about 3 mGal. This corresponds to radar altimeter slope errors of better than 3 μrad or radar altimeter quasi-geoid height difference standard deviations of 6 mm. This is very challenging and likely not feasible. In reality, radar altimetry provides the mean sea surface slopes, which may differ from the quasi-geoid slopes. Hence, a slope correction is needed, which poses constraints on the accuracy of water levels from a hydrodynamic model (e.g., *Holt et al., 2005*; *Zijl et al., 2013*). Finally, there will always be a stroke along the coast of 5–10 km width void of radar altimeter data of sufficient accuracy (e.g., *Andersen and Knudsen, 2000*; *Deng et al., 2002*). This gap needs to be filled to avoid distortions in the quasi-geoid, which may also propagate onto land inwards.

In view of this, we consider airborne gravimetry as the only, currently available, data acquisition technique that can provide a data coverage and accuracy at sea that meets the requirements of a 5-mm quasi-geoid. State-of-the-art sensor systems can provide under ideal conditions (e.g., low turbulence, appropriate aircraft, smooth spatial gravity variations, low flight speed, and low elevations) an accuracy of 1 mGal at 5 km half wavelength spatial resolution (e.g., *Hannah, 2001*; *Bruton et al., 2002*; *Studinger et al., 2008*). This is sufficient for the realization of a 5-mm quasi-geoid for the Netherlands (cf. Figs 8 and 9).

6. CONCLUSIONS

The goal of this study was to assess the gravity data requirements in terms of commission and omission errors for a desired (i.e. target) accuracy of the quasi-geoid for the Netherlands mainland and continental shelf . The commission and omission errors are the errors in the quasi-geoid model caused by noise in the data and the limited spatial resolution of the data, respectively. The target accuracy was set to 5-mm standard deviation at 68% confidence level. Four questions were formulated and answered in this study:

1. How does the omission error change as function of the spatial resolution of the gravity data set for the Netherlands mainland and continental shelf?
   Answer: The omission error strongly depends on the roughness of the land topography and bathymetry. For the Netherlands continental shelf and Central and Northern Netherlands, it can be modeled as $\varepsilon_{om}\left[\mathrm{mm}\right]=0.32d$, where d is the data spacing in units of kilometres. For the more hilly Southern Netherlands, this error can be modelled as $\varepsilon_{om}\left[\mathrm{mm}\right]=0.92d$.
2. How large is the commission error as function of the noise standard deviation of the gravity data assuming white Gaussian noise?
   Answer: Assuming that the contribution of GGM to the commission error is negligible, the commission error depends on the kernel modification, the data spacing, and the noise standard deviation of the surface gravity data set. It does not depend on the location or any other parameter. Assuming that a spheroidal Stokes kernel is used, it can be modeled as $\sigma_{om}\left[\mathrm{mm}\right]=0.277d\sigma_{\Delta g}$, where $\sigma_{\Delta g}$ is the noise standard deviation of the surface gravity anomaly data set in units of mGal. The commission error of state-of-the-art GGMs increases exponentially with the maximum degree and decreases with increasing latitude. For GOCO05S, an upper limit of the commission error over the Netherlands mainland is provided by the model $\sigma_{\mathrm{GGM}}\left[\mathrm{mm}\right]=\exp\left(0.03676L-11.419\right)$, where L is the maximum degree up to which GOCO05S is used in the remove-compute-restore approach. Only if the GGM is truncated at a sufficiently low degree, its contribution to the (total) commission error can be neglected. For GOCO05S, a maximum degree of 100 contributes to the overall commission error with about 0.4 mm. At degree 200, this increases to about 14 mm. We do not expect a significant improvement of the GGMs in the next few years.

3. What density of the gravity data and what data accuracy are needed to ensure a 5-mm quasi-geoid (68% confidence level) for the Netherlands?
   Answer: Assuming that the spheroidal Stokes kernel is used, the total error at the 68% confidence level can be modeled as $\sigma\left[\text{mm}\right] = d\left(0.32 + 0.277\sigma_{\Delta g}\right)$ for the Netherlands continental shelf as well as the Central and Northern Netherlands and $\sigma\left[\text{mm}\right] = d\left(0.92 + 0.277\sigma_{\Delta g}\right)$ for the Southern Netherlands. Therefore, assuming a standard deviation of 1.5 mGal for the surface gravity anomaly data set, which is a level of accuracy that the currently available surface data sets used to compute the Netherlands quasi-geoid fulfill, a data spacing of about 3.5 km (for the Southern Netherlands) and about 6.5 km (for Netherlands continental shelf and Central and Northern Netherlands) are sufficient for a 5-mm quasi-geoid.
4. To what extent do the currently available gravity data sets meet the requirements for a 5-mm quasi-geoid? If not, is there a data acquisition technique that is able to provide a data set with the necessary accuracy and density?
   Answer: Based on the assumption of white noise in data and no systematic errors, the currently available GGMs and terrestrial gravity anomaly data sets fulfill the requirements for a 5-mm quasi-geoid for the Netherlands in terms of density and accuracy. The marine gravity anomaly data set fails to do so. Though the quality of the radar altimeter-derived data set will improve in the future when Sentinel data are used, this improvement will not be sufficient. Moreover, the quality of those data will be insufficient in a stroke of a few kilometres off the coast. Shipboard gravimetry provides data with sufficient accuracy, but is too expensive seen the requirements in terms of spatial resolution. The only available and at the same time cost effective acquisition technique that is able to provide the gravity data at sea with sufficient density and spatial resolution is airborne gravimetry.

Acknowledgements: The study was financed by the ministry of Infrastructure and the Environment, Rijkswaterstaat in the Netherlands. Hassan H. Farahani acknowledges financial support provided by the Dutch Technology Foundation STW in the framework of the Netherlands Vertical Reference Frame (NEVREF) project. The gravity data sets used in this study were provided by a number of institutions: British Geological Service, Bundesamt für Kartographie und Geodäsie (Germany), Institut für Erdmessung of the Leibniz University Hannover, Bureau Gravimétrique International, Banque de données Gravimétriques de la France, and Bureau de Recherches Géologiques et Minières. We are thankful to Christopher Jekeli for valuable discussions. We thank Nico Sneeuw and two anonymous reviewers for their constructive remarks and corrections, which helped us to improve the quality of the manuscript.

References

Andersen O.B. and Knudsen P., 2000. The role of satellite altimetry in gravity field modelling in coastal areas. *Phys. Chem. Earth*, **25**, 17–24, DOI: 10.1016/S1464-1895(00)00004-1.

Ågren J. and Sjöberg L.E., 2014. Investigation of gravity data requirements for a 5 mm-quasigeoid model over Sweden. In: Marti U. (Ed.), *Gravity, Geoid and Height Systems*. International Association of Geodesy Symposia 141, Springer-Verlag, Heidelberg, Germany, 143–150, DOI: 10.1007/978-3-319-10837-7_18.

Bruton A.M., Schwarz K.P., Ferguson S., Kern M. and Wei M., 2002. Deriving acceleration from DGPS: toward higher resolution applications of airborne gravimetry. *GPS Solut.*, **5**, 1–14, DOI: 10.1007/PL00012894.

Deng X., Featherstone W.E., Hwang C. and Berry P.A.M., 2002. Estimation of contamination of ERS-2 and Poseidon satellite radar altimetry close to the coasts of Australia. *Mar. Geod.*, **25**, 249–271, DOI: 10.1080/01490410214990.

Eicker A., 2008. *Gravity Field Refinement by Radial Basis Functions from In-Situ Satellite Data.* Ph.D. Thesis. University of Bonn, Bonn, Germany (http://hss.ulb.uni-bonn.de/2008/1375).

EuroGeographics, 2008. *EuroDEM Product Description* (www.eurogeographics.org).

Farahani H.H., Slobbe D.C., Klees R. and Seitz K., 2017. Impact of accounting for coloured noise in radar altimetry data in regional quasi-geoid modelling. *J. Geodesy*, **91**, 97–112, DOI: 10.1007/s00190-016-0941-6.

Farr T.G., Rosen P.A., Caro E., Crippen R., Duren R., Hensley S., Kobrick M., Paller M., Rodriguez E., Roth L., Seal D., Shaffer S., Shimada J., Umland J., Werner M., Oskin M., Burbank D. and Alsdorf D., 2007. The Shuttle Radar Topography Mission. *Rev. Geophys.*, **45**, RG2004, DOI: 10.1029/2005RG000183.

Forsberg R., 1984. *A Study of Terrain Reductions, Density Anomalies and Geophysical Inversion Methods in Gravity Field Modeling*. Technical Report 5, Ohio State University, Columbus, Ohio, USA.

Forsberg R., 1985. Gravity field terrain effect computations by FFT. *Bull. Geod.*, **59**, 342–360, DOI: 10.1007/BF02521068.

Forsberg R., 1993. Modelling the fine-structure of the geoid: methods, data requirements and some results. *Surv. Geophys.*, **14**, 403–418, DOI: 10.1007/BF00690568.

Hannah J., 2001. *Airborne Gravimetry: A Status Report*. Department of Surveying, University of Otago, Dunedin, New Zealand (http://citeseerx.ist.psu.edu/viewdoc/download?doi=10.1.1.557.3430&rep=rep1&type=pdf).

Heck B., 1990. An evaluation of some systematic error sources affecting terrestrial gravity anomalies. *Bull. Geod.*, **64**, 88–108, DOI: 10.1007/BF02530617.

Heiskanen W.A. and Moritz H., 1967. *Physical Geodesy*. Freeman W.H., New York, N.Y.

Hirt C., Claessens S., Fecher T., Kuhn M., Pail R. and Rexer M., 2013. New ultrahigh-resolution picture of Earth's gravity field. *Geophys. Res. Lett.*, **40**, 4279–4283, DOI: 10.1002/grl.50838.

Holt J.T., Allen J.I., Proctor R. and Gilbert F., 2005. Error quantification of a high-resolution coupled hydrodynamic-ecosystem coastal-ocean model: Part 1 model overview and assessment of the hydrodynamics. *J. Mar. Syst.*, **57**, 167–188, DOI: 10.1016/j.jmarsys.2005.04.008.

Jekeli C., 1981. Modifying Stokes' function to reduce the error of geoid undulation computations. *J. Geophys. Res.*, **86**, 6985–6990, DOI: 10.1029/JB086iB08p06985.

Jekeli C., 2012. Omission error, data requirements, and the fractal dimension of the geoid. In: Sneeuw N., Nová P., Crespi M. and Sansò F. (Eds), *VII Hotine-Marussi Symposium on Mathematical Geodesy*. International Association of Geodesy Symposia, **137**, 181–187, Springer-Verlag, Berlin, Germany, DOI: 0.1007/978-3-642-22078-4_27.

Jekeli C., Yang H.J. and Kwon J.H., 2009. Using gravity and topography-implied anomalies to assess data requirements for precise geoid computation. *J. Geodesy*, **83**, 1193–1202, DOI: 10.1007/s00190-009-0337-y.

Kaula W.M., 1966. *Theory of Satellite Geodesy: Applications of Satellites to Geodesy*. Dover Publications, Mineola, N.Y., ISBN: 9780486152219.

Kearsley A.H.W., 1986. Data requirements for determining precise relative geoid heights from gravimetry. J. Geophys. Res., **91(B9)**, 9193–9201, DOI: 10.1029/JB091iB09p09193.

Klees R., Prutkin I., Tenzer R. and Wittwer T., 2007. *Development of a Technique for Combining Parameters of the Earth's Gravity Field for Quasi-Geoid Determination on the Territory of the Federal Republic of Germany and Europe*. Delft University Press, DUP Science, Delft, The Netherlands.

Klees R., Tenzer R., Prutkin I. and Wittwer T., 2008. A data-driven approach to local gravity field modelling using spherical radial basis functions. *J. Geodesy*, **82**, 457–471, DOI: 10.1007/s00190-007-0196-3.

Mayer-Gürr T., Pail R., Gruber T., Fecher T., Rexer M., Schuh W.-D., Kusche J., Brockmann J.-M., Rieser D., Zehentner N., Kvas A., Klinger B., Baur O., Höck E., Krauss S. and Jäggi A., 2015. The combined satellite gravity field model GOCO05S. *Geophys. Res. Abs.*, **17**, EGU2015-12364.

de Min E., 1996. *De geoïde voor Nederland (The Geoid for the Netherlands)*. Ph.D. Thesis. Delft University of Technology, Netherlands Geodetic Commission 34, Delft, The Netherlands, ISBN-13: 9789061322573, ISBN-10: 906132257X.

Moritz H., 1978. Least-squares collocation. *Rev. Geophys.*, **16**, 421–430, DOI: 10.1029 /RG016i003p00421.

Moritz H., 1984. Geodetic reference system 1980. *Bull. Geod*., **54**, 395–405, DOI: 10.1007 /BF02521480.

Novák P., Vaníček P., Véronneau M., Holmes S. and Featherstone W., 2001. On the accuracy of modified Stokes' integration in high-frequency gravimetric geoid determination. *J. Geodesy*, **74**, 644–654, DOI: 10.1007/s001900000126.

Pail R., Goiginger H., Schuh W.-D., Höck E., Brockmann J.M., Fecher T., Gruber T., Mayer-Gürr T., Kusche J., Jäggi A. and Rieser D., 2010. Combined satellite gravity field model GOCO01S derived from GOCE and GRACE. *Geophys. Res. Lett.*, **37**, L20314, DOI: 10.1029/2010GL044906.

Sandwell D.T. and Smith W.H.F., 1997. Marine gravity anomaly from Geosat and ERS-1 satellite altimetry. *J. Geophys. Res.*, **102**, 10039–10054, DOI: 10.1029/96JB03223.

Schmidt M., Fengler M., Mayer-Gürr T., Eicker A., Kusche J., Sánchez L. and Han S.-C., 2007. Regional gravity modeling in terms of spherical base functions. *J. Geodesy*, **81**, 17–38, DOI: 10.1007/s00190-006-0101-5.

Sjöberg L.E., 2003. A solution to the downward continuation effect on the geoid determined by Stokes' formula. *J. Geodesy*, **77**, 94–100, DOI: 10.1007/s00190-002-0306-1.

Sjöberg L.E., 2004. The effect on the geoid of lateral topographic density variations. *J. Geodesy*, **78**, 34–39, DOI: 10.1007/s00190-003-0363-0.

Slobbe D.C., 2013. *Roadmap to a Mutually Consistent Set of Offshore Vertical Reference Frames*. Ph.D. Thesis. Delft University of Technology, Netherlands Geodetic Commission 82, Delft, The Netherlands, ISBN: 9789061323440.

Slobbe D.C. and Klees R., 2014. The impact of the dynamic sea surface topography on the quasi-geoid in shallow coastal waters. *J. Geodesy*, **88**, 241–261, DOI: 10.1007/s00190-013-0679-3.

Slobbe D.C., Klees R. and Gunter B.C., 2014. Realization of a consistent set of vertical reference surfaces in coastal areas. *J. Geodesy*, **88**, 601–615, DOI: 10.1007/s00190-014-0709-9.

Smith W.H.F., 2010. The marine geoid and satellite altimetry. In: Barale V., Gower J.F.R. and Alberotanza L. (Eds), *Oceanography from Space*. Springer Science+Business Media B.V., Dordrecht, The Netherlands, 181–193, DOI: 10.1007/978-90-481-8681-5_11.

Studinger M., Bell R. and Frearson N., 2008. Comparison of AIRGrav and GT-1A airborne gravimeters for research applications. *Geophysics*, **73**, I51–I61, DOI: 10.1190/1.2969664.

Tscherning C.C., 1978. Collocation and least squares methods as a tool for handling gravity field dependent data obtained through space research techniques. *Bull. Geod.*, **52**, 199–212, DOI: 10.1007/BF02521773

Tscherning C.C., 1985. Geoid modelling using collocation in Scandinavia and Greenland. *Mar. Geod.*, **9**, 1–16, DOI: 10.1080/15210608509379512.

Turcotte D.L., 1987. A fractal interpretation of topography and geoid spectra on the Earth, Moon, Venus, and Mars. *J. Geophys. Res.*, **92(B4)**, E597–E601, DOI: 10.1029/JB092iB04p0E597.

Vaníček P., Castle R.O. and Balazs E.I., 1980. Geodetic leveling and its applications. *Rev. Geophys.*, **18**, 505–524, DOI: 10.1029/RG018i002p00505.

Vaníček P. and Krakiwsky E.J., 1986. *Geodesy: The Concepts*. 2nd Edition. Elsevier Science, Amsterdam, The Netherlands, ISBN: 9780444877758.

Vaníček P. and Kleusberg A., 1987. The Canadian geoid - Stokesian approach. *Manus. Geod.*, **12**, 86–98.

Vaníček P., Huang J., Novák P., Pagiatakis S., Véronneau M., Martinec Z. and Featherstone W.E., 1999. Determination of the boundary values for the Stokes-Helmert problem. *J. Geodesy*, **73**, 180–192, DOI: 10.1007/s001900050235.

Véronneau M. and Huang J., 2016. The Canadian Geodetic Vertical Datum of 2013 (CGVD2013). *Geomatica*, **70**, 9–19, DOI: 10.5623/cig2016-101.

Wittwer T., 2009. *Regional Gravity Field Modelling with Radial Basis Functions*. Ph.D. Thesis. Delft University of Technology, Netherlands Geodetic Commission 72, Delft, The Netherlands, ISBN: 9789061323150.

Zijl F., Verlaan M. and Gerritsen H., 2013. Improved water-level forecasting for the Northwest European Shelf and North Sea through direct modelling of tide, surge and non-linear interaction. *Ocean Dyn.*, **63**, 823–847, DOI: 10.1007/s10236-013-0624-2.